The Snake Origins*

Olivier ECABERT

Institut für Nachrichtentechnik, TU Darmstadt,
D-64283 Darmstadt, Germany

January 24, 2000

Abstract

Active contours (snakes) provide a unified account of a number of visual problems, including detection of edges, lines and subjective contours as well as motion tracking and stereo matching. Since their first apparition the researchers of the image processing community have simply applied this model to their problems without explaining where its parameters come from nor how to obtain its motion equations. To get a reality-based interpretation of the *classic* snake parameters (i.e. elasticity and bending, also referred to as α and β) we propose an approach originates from the theory of the elasticity. Then we derive the motion equations from the variational method and we finally give some examples of segmentation. An alternative way of computing the external force field which increases the performance of snakes in presence of concavities is studied. We finally propose a new approach based on the dynamic modification of β that improves the snake behavior at corners.

1 Introduction

In 1987, Kass *et al.* [4] introduced a new approach for locating features of interest in images. This model, commonly called *snake*, is based on the energy minimizing of an active contour. The snake energy may be decomposed in two terms: The external and internal energy. The external energy is represented by external constraint forces and by image forces that pull the snake toward features such as line, edges or other features of interest. The internal energy allows representing the snake as a continuous curve whose shape is controlled by internal continuity forces which act as a smoothness constraint. Two type of forces are usually considered: The elasticity force which holds the curve together and the bending force which prevents the snake bending too much.

A traditional snake may be considered as a curve $\mathbf{v}(s,t) = (x(s,t), y(s,t))'$, with s a spatial parameter and t a time parameter, which moves through the spatial domain of an image minimizing the potential energy functional

$$E = \int E_{snake}(\mathbf{v}(s,t))ds = \int E_{int}(\mathbf{v}(s,t)) + E_{ext}(\mathbf{v}(s,t))ds \tag{1}$$

where E_{int} represents the internal energy of the snake and E_{ext} the external energy derived from the image, so that it takes its smaller values at the features of interest (e.g. boundaries, edges, ...). According to [10] and given a gray-level image $I(x,y)$,

*A part of this work was done at the Signal Processing Laboratory, Swiss Federal Institute of Technology (January 10 - 21, 2000) in collaboration with J.-P. Thiran and F. Mendels.

viewed as a function of continuous variables (x, y), typical external energies designed to lead an active contour toward step edges are

$$E_{ext}^{(1)}(x,y) = -|\nabla I(x,y)|^2$$

and

$$E_{ext}^{(2)}(x,y) = -|\nabla [G_\sigma(x,y) * I(x,y)]|^2$$

where $G_\sigma(x,y)$ is a two-dimensional Gaussian function with standard deviation σ and ∇ the gradient operator. If the image is a line drawing (black on white), then appropriate external energies include

$$E_{ext}^{(3)}(x,y) = I(x,y)$$

and

$$E_{ext}^{(4)}(x,y) = G_\sigma(x,y) * I(x,y).$$

The internal energy in (1) can be defined as follow [4]:

$$E_{int}(\mathbf{v}(s)) = \frac{1}{2}[\alpha(s)|\frac{\partial \mathbf{v}(s)}{\partial s}|^2 + \beta(s)|\frac{\partial^2 \mathbf{v}(s)}{\partial s^2}|^2] \tag{2}$$

The internal potential energy is composed of a first-order term controlled by $\alpha(s)$ and a second-order term controlled by $\beta(s)$. The first-order term makes the snake behave like a string (i.e. resists stretching), whereas the second-order term makes it act like a rod (i.e. resists bending). For example in a spline description of the curve, setting $\beta(s)$ to zero at a point allows the snake to become second-order discontinuous and develop a corner.

The usual method used to minimize (1) consists in solving its Euler-Lagrange equations making the snake dynamic by converting its potential energy to kinetic energy through an energy dissipation function (see for example [5] or [10]).

Although many authors use this scheme to solve their problems, none of them explain how (2) is derived neither whether the parameters of the snake (α and β) are related with some physical interpretation. In Section 2, we give a complete derivation for α and β based on the theory of the elasticity and the mechanics of the deformable solid. We show that these parameters are strongly related with physical values such as the Young modulus, the tension force,... In Section 3 we first introduce the concept of variations and we then derive the Euler-Lagrange as well as the motion equations of the snake. Some examples of segmentation are finally given in Section 4. In this Section, we also propose some improvements of the original method in order that the snake better converges on the features of interest. We especially replace the external forces with the gradient vector flow (cf. [10]) and propose a new approach that improves the performance of the snake in presence of corners.

2 The Parameters α and β of the Snake

In this section we answer the question: Where do the stretching and bending parameters of the snake (i.e. α and β) come from and how are they related with some physical reality? For that purpose, we need information from the theory of elasticity and from the mechanics of the deformable solid. Both topics are usually not familiar to the people coming from the signal processing community and although we try simplifying the problem and being as complete as possible, the reader may need more information. In that case we recommend him the excellent references [7] and [3].

2.1 Principle of Superposition

As in the signal and system theory, the principle of superposition is valid in elasticity under some assumptions. This property is very useful since the complete but complicated motion of a deformable solid can be expressed as the superposition of several elementary motions that are simpler to analyze. In our case, the snake is considered to be a deformable curve which is a function of the x and y coordinates only - and not the z or height - since we wish the snake to stick to the potential surface (embedded in $\Re^3$). Thus, unconstrained movement along the third spatial dimension (i.e. height) is required. Hence we permit the snake to have two deformational degrees of freedom in the plane, that is, in the x, y coordinates. A direct consequence to this, is that the internal energy term of the snake will not depend on torsion and that second-order derivatives will be sufficient [5]. Moreover the snake can be thought of as a beam with a cross section which tends towards zero. To describe the motion of the snake and according to these assumptions it suffices to analyze two elementary motions:

- Deflection of an elastic string
- Deflection of the central line of a beam.

2.2 Deflection of an Elastic String

Let a string (i.e. a rod with a cross section equal to zero) be stretched by a uniformly distributed tension force T and placed in a referential as shown in Figure 1. The

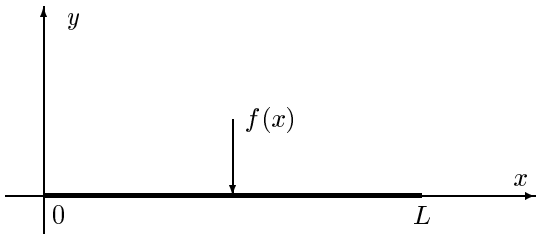

Figure 1: Deflected String by a Distributed Transverse Load $f(x)$.

string is deflected by a distributed transverse load $f(x)$ per unit of the string. We suppose that the transverse deflection $y(x)$ is small and the change in the stretching force T produced by the deflection is negligible. It means that the tension force after deflection is still given by T. In the case of the snake, this deflection may be seen as a modification of the surface of the image where the snake (string) lies. A hole in the image (i.e. where the pixel values are weak) acts as if a deflection $f(x)$ pushed down the snake (the snake is attracted down under the influence of the gravitational force). On the other hand, a small hill in the image acts as if a deflection $f(x)$ pushed up the snake.

In these conditions it is possible to calculate the internal energy of the string. This energy is also referred to as the *strain energy* U_1. It is equivalent to the work of the stretching force T all along the string. If the stretch of the string is referred to as e and the curve parameter along the deformed string as s, we have

$$U_1 = \int dW = \int T\, de = T \int (ds - dx) = \int (\sqrt{1 + (y')^2} - 1)\, dx.$$

Since we are dealing with the linear theory, $(y')^2 \ll 1$ and we finally get

$$U_1 = \frac{1}{2} T \int (y')^2 \, dx. \tag{3}$$

2.3 Deflection of the Central Line of a Beam

In this section we are going to derivate the terms related with the curvature of the snake. For that purpose, the deflection of the central line of a beam is analyzed. It is justified to only consider the central line of a beam since the snake correspond to the limit of the beam when its surface tends toward zero. When the beam reaches this limit, it is only compose of its central line.

Let the axis of a beam of constant cross section coincide with the x-axis, and suppose that the beam is bent by a transverse load $p = f(x)$ estimated per unit length of the beam. The static equations will be established according to the notations of the Figure 2. Moreover we suppose the assumption of Bernoulli valid. It

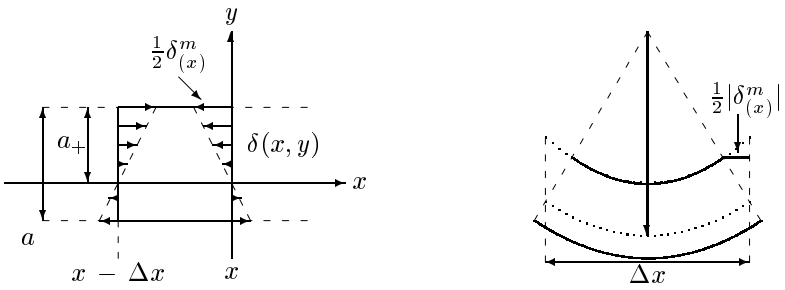

Figure 2: Part of the beam limited by its cross sections situated in $\Delta x - x$ and x. (a) before the deformation, (b) after the deflection. On that figure, $\delta^m(x)$ is negative.

means that the cross sections remain plane after deformation and thus the "fibers" of the beam remain parallel respective to x. After deflection, the fiber length is $\Delta\, x + \delta(\Delta\, x)$, with

$$\delta(\Delta\, x) = \delta(x, y) = \delta^m(x) \frac{y}{a_+}.$$

$\delta^m(x)$ is the maximal (respectively minimal) stretching of the fiber in y, when its initial length is Δx. For the small deflections (elastic deformations), the Hook's law says that the tensile stress σ_{11} at a point (x, y) is proportional to the stretch ε_{11} at this same point

$$\varepsilon_{11} = \frac{\delta(x,y)}{\Delta x} = \varepsilon^m_{11} \frac{y}{a_+}; \qquad \varepsilon^m_{11} = \frac{\delta^m(x)}{\Delta x}$$

$$\Rightarrow \sigma_{11}(x,y) = E\varepsilon_{11}(x,y) = \sigma^m(x) \frac{y}{a_+}$$

where E is the elasticity modulus and $\sigma^m(x) = E\frac{\delta^m(x)}{\Delta x}$. Since the tensile stress is known the bending moment of the beam can be expressed as

$$M = -\int \sigma_{11}(x,y) y \, dS_1 = -\frac{1}{a_+} \sigma^m \int y^2 \, dS_1$$

or equivalently

$$\sigma^m = -\frac{a_+}{I} \cdot M$$

with $I = \int_{\Sigma_1} y^2 \, dS_1$. It is called moment of inertia of the cross section Σ_1 respective to the z-axis. And from the Hook's law we have

$$\varepsilon^m = \frac{\sigma^m}{E} = -\frac{M a_+}{IE}.$$

Moreover it can be shown [7] that the strain energy density W is given by

$$W = \frac{1}{2}\sigma^m \varepsilon^m$$

and thus

$$W = \frac{M^2 y^2}{2EI^2}. \tag{4}$$

The strain energy per unit length is obtained by integrating (4) over the cross section of the beam

$$\int_{\Sigma_1} W \, dS_1 = \frac{M^2}{2EI^2} \int_{\Sigma_1} y^2 \, dS_1 = \frac{M^2}{2EI}. \tag{5}$$

To go a step further, we have to express the inertia moment M as a function of the curvature radius ρ of the beam. From Figure 2 we have

$$\frac{\Delta x}{2} \cdot \frac{1}{\rho(x)} = -\frac{\delta^m(x)}{2a_+}$$

$$\frac{1}{\rho(x)} = -\frac{\delta^m(x)}{\Delta x \, a_+} = \frac{\varepsilon^m_{11}}{a_+} = -\frac{\sigma^m}{a_+ E} = \frac{a_+ M}{I a_+ E} = \frac{M}{EI}. \tag{6}$$

On the other hand, [9] shows that the radius of curvature ρ of the curve $y = y(x)$ is given by

$$\frac{1}{\rho} = \frac{y''}{(1 + y'^2)^{\frac{3}{2}}}. \tag{7}$$

Then replacing ρ in (6) with its expression in (7) and assuming that we are still dealing with the linear theory $(y')^2 \ll 1$, it yields

$$y'' = \frac{M}{EI}$$

and thus from (5)

$$\int_{\Sigma_1} W \, dS_1 = \frac{1}{2} E \, I \, (y'')^2.$$

To obtain the total strain energy U_2 it suffices now to integrate the above relation all along the beam

$$U_2 = \frac{1}{2} E \, I \int (y'')^2 \, dx. \tag{8}$$

2.4 Parameter Interpretation

The results of the previous sections can be easily extended to the two dimensional case. Indeed a snake is usually represented as a curve of two variables in the plane and each of theses variables is also a function of a same parameter as described in Section 1. Substituting in (3) and (8) x, respectively y for s, respectively $\mathbf{v}$ and using the property of superposition, this yields for the total strain energy U of the snake

$$U = \int E_{int}\, ds = U_1 + U_2 = \frac{1}{2}\int (T|\mathbf{v}'(s)|^2 + EI|\mathbf{v}''(s)|^2)\, ds. \tag{9}$$

Identifying (9) with the internal energy (2) it is easy to see how the two parameters of the snake are related with the different physical values, that is

$$\boxed{\begin{array}{c}\alpha = T \\ \beta = EI.\end{array}} \tag{10}$$

- α is equal to the tension force in the snake. Thus, the bigger α, the bigger the stretching force, so that the snake resists more the stretching. It agrees with the results published in the literature (see for example [4] or [5]). If α is big the snake tends to shrink and have an intrinsic bias toward solutions that reduce its length.

- β is equal to the product of the elasticity modulus E and the inertia moment I of the snake cross section. The elasticity modulus is the proportional coefficient between the tensile stress and the stretch of a deformable solid. If E is weak, a small tensile stress will produce a great amount of stretch deformation. Moreover the radius of the cross section will be reduced in the same proportion. Thus a material with a great E better resists the tensile stress than a material with a small elasticity modulus.

  On the other hand, the inertia moment of beam is related with its resistance to the bending. I is usually used to increase the resistance of a beam without changing its material (and thus E). The bigger I, the better the beam resists the bending.

  In our *ideal* case, the snake has a cross section which tends towards zero, thus the inertia moment tends towards zero too. It means that to have a non zero β $(= EI)$, i.e. a snake which resists the bending, the elasticity modulus must tend towards infinity! It is obvious since we have an infinitely thin material which have to resist the bending.

3 The Euler-Lagrange and Motion Equations

The Euler-Lagrange equations of the snake, i.e. the equations which describes the curve and satisfies (1) can be obtained from the theory of the variations. To derive the Euler-Lagrange equations of the snake we follow the same framework as proposed in [1].

3.1 An Example by Way of Introduction

Let the material point P, rolling without friction along the curve C from the point $P_0(x_0, y_0)$ to $P_1(x_1, y_1)$, be under the influence of the gravitational force only. The gravitational force is oriented along the y-axis as shown in Figure 3. From the principle of energy conservation

$$\frac{m}{2}\, v^2 = mgy$$

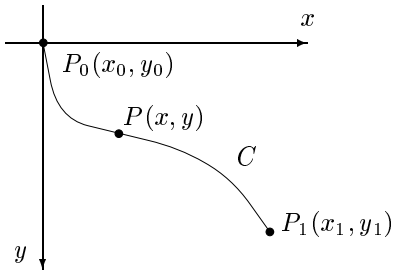

Figure 3: Material point P rolling along the curve C without friction.

we can calculate the velocity for any time t

$$v = \frac{ds}{dt} = \sqrt{2gy}$$

where s is a spatial parameter that describes the curve. The time T that the point needs to go from P_0 to P_1 along the curve C is given by

$$T = \int_C dt = \int_C \frac{dt}{ds}\, ds = \int_C \frac{1}{v}\, dt$$

with $ds = \sqrt{1 + y'^2}\, dx$. Thus

$$T = \int_{x_0}^{x_1} \frac{\sqrt{1 + y'^2}}{\sqrt{2gy}}\, dx. \tag{11}$$

How should the curve C be chosen in order that the travel of the point be as short as possible? In other words: What is the function among all the functions $y(x)$ which satisfies the boundaries $y(0) = y_0$ and $y(1) = y_1$ and which minimizes (11)? The fundamental problem of variational methods usually consists in finding the extremal value of an integral which represents a physical quantity.

3.2 Euler-Lagrange Equations

As in the previous section, we consider here only the one dimensional case. The extension towards a more generalized curve in the plane is straightforward (see Section 2.4). In order to study the variational method we look for a function $y(x)$ satisfying the boundary conditions $y(x_0) = y_0$ and $y(x_1) = y_1$ so that the integral

$$I = \int_{x_0}^{x_1} F(x, y(x), y'(x), y''(x))\, dx \tag{12}$$

has an extremum. F is an arbitrary function and we assume that I is well defined. Moreover we also suppose that $y(x)$ is at least continuously derivative up to the third order. Let's define the function $\tilde{y}(x) = y(x) + \epsilon\eta(x)$, where $\eta(x)$ is any arbitrary function with the boundary conditions:

$$\eta(x_0) = \eta(x_1) = \eta'(x_0) = \eta'(x_1) = 0 \tag{13}$$

and ϵ a parameter. Replacing $y(x)$ for $\tilde{y}(x)$ in (12), we have

$$I(\epsilon) = \int_{x_0}^{x_1} F(x, y(x) + \epsilon\eta(x), y'(x) + \epsilon\eta'(x), y''(x) + \epsilon\eta''(x))\, dx. \tag{14}$$

Since $y(x)$ is an extremum of (12), the function $I(\epsilon)$ must have an extremum for $\epsilon = 0$ and thus its first derivative vanishes for $\epsilon = 0$. Derivating (14) respective to ϵ, we have

$$\begin{aligned} I'(0) = 0 = \int_{x_0}^{x_1} [\frac{\partial F(x, y, y', y'')}{\partial y}\eta(x) + \frac{\partial F(x, y, y', y'')}{\partial y'}\eta'(x) + \\ \frac{\partial F(x, y, y', y'')}{\partial y''}\eta''(x)], dx. \end{aligned} \tag{15}$$

After integrating by parts once the second term of (15) and twice the third term, and using the boundary conditions (13) we get

$$I'(0) = \int_{x_0}^{x_1} \eta(x) \left[\frac{\partial F}{\partial y} - \frac{d}{dx}\left(\frac{\partial F}{\partial y'}\right) + \frac{d^2}{dx^2}\left(\frac{\partial F}{\partial y''}\right)\right] = 0 \tag{16}$$

The coefficient of $\eta(x)$ under the integral (16) must be zero in order that (16) holds. Indeed, $\eta(x)$ may be any function and for example it could be chosen such as it is equal to 1 when its coefficient is positive and equal to -1 when its coefficient is negative. Thus

$$\frac{\partial F}{\partial y} - \frac{d}{dx}\left(\frac{\partial F}{\partial y'}\right) + \frac{d^2}{dx^2}\left(\frac{\partial F}{\partial y''}\right) = 0. \tag{17}$$

This equation is called Euler-Lagrange equation.

In the case of the snake, we have

$$F(s, \mathbf{v}(s), \mathbf{v}'(s), \mathbf{v}''(s)) = E_{snake} = E_{int} + E_{ext} =$$

$$\frac{1}{2}[\alpha(s)|\frac{\partial \mathbf{v}(s)}{\partial s}|^2 + \beta(s)|\frac{\partial^2 \mathbf{v}(s)}{\partial s^2}|^2] + E_{ext}(\mathbf{v}(s)). \tag{18}$$

This yields

$$\frac{d}{ds}(\alpha(s)\mathbf{v}'(s)) - \frac{d^2}{ds^2}(\beta(s)\mathbf{v}''(s)) - \nabla E_{ext}(\mathbf{v}(s)) = 0. \tag{19}$$

3.3 Motion Equations

Equation (19) can be viewed as a force balance equation

$$\mathbf{F}_{int} + \mathbf{F}_{ext}^{(p)} = 0. \tag{20}$$

(20) describes the static state of the snake. If we want to express the dynamic comportment of the snake, (20) must be rewritten

$$\mathbf{F}_{int} + \mathbf{F}_{ext}^{(p)} + \mathbf{F}^{(nc)} = \mu\frac{\partial^2 \mathbf{v}}{\partial t^2}. \tag{21}$$

where μ is the mass density, $\frac{\partial^2 \mathbf{v}}{\partial t^2}$ the acceleration vector and $\mathbf{F}^{(nc)}$ represents the non conservative forces which dissipate the kinetic energy and stabilize the snake. They are given by

$$\mathbf{F}^{(nc)} = -\gamma\frac{\partial \mathbf{v}}{\partial t}$$

with γ a constant damping coefficient or viscosity factor. To be as close of the physics as possible, we can rewrite the expression of the external energy as $E'^{(i)}_{ext}(x,y) = \mu\,\mathcal{G}\,E^{(i)}_{ext}(x,y)$, where $\mathcal{G}$ is equivalent to a gravitational constant to give more or less importance to the external forces and $E^{(i)}_{ext}(x,y)$ is one of the energies defined in Section 1. Finally the motion equations for both coordinates x and y are

$$\mu\frac{\partial^2 x}{\partial t^2} + \gamma\frac{\partial x}{\partial t} - \frac{\partial}{\partial s}(\alpha(s)\frac{\partial x}{\partial s}) + \frac{\partial^2}{\partial s^2}(\beta(s)\frac{\partial^2 x}{\partial s^2}) = -\mu\mathcal{G}\frac{\partial E'^{(i)}_{ext}}{\partial x} \tag{22.a}$$

and

$$\mu\frac{\partial^2 y}{\partial t^2} + \gamma\frac{\partial y}{\partial t} - \frac{\partial}{\partial s}(\alpha(s)\frac{\partial y}{\partial s}) + \frac{\partial^2}{\partial s^2}(\beta(s)\frac{\partial^2 y}{\partial s^2}) = -\mu\mathcal{G}\frac{\partial E'^{(i)}_{ext}}{\partial y}. \tag{22.b}$$

This system of partial differential equations may be solved with a classical method of numerical integration such as finite differences or finite elements. For the numerical implementation we followed the work done by Leymarie and Levine in [5].

4 Examples and Improvement of the Basic Model

In Subsection 4.1, many examples of edge detection in different situations will be investigated. We present first some images where the snake well behaves in order to show that the basic snake may also be robust and very effective in some situations. Then we give some examples which emphasize the limitations of our basic model. In Subsections 4.2 and 4.3 improvements of the basic snake are proposed in order to correct some of its primary weaknesses.

4.1 Basic Model

The first example consists in segmenting the coin situated in the lower left corner of Figure 4. This is a quite simple situation since the different coins are well isolated from one to another. Moreover no additive noise is present in the image. The result of the segmentation is given in Figure 4 with the following parameters: $\alpha = 3$, $\beta = 2$, $\gamma = 2$, $\Delta t = 0.5$, $\mu = 1$, $\mathcal{G} = 5$. The *snaxel* length was kept at 1 pixel by resampling of the snake during the convergence by dynamic reparameterization of the snake as described in [6]

In the next example, the same coin is segmented, but some Gaussian noise was added to the image (see Figure 5 (a)). The signal-to-noise ratio (SNR) of the image is equal to 12 dB. In that case, only 6 discrete points were placed around the coin to be segmented. This coarse initial contour is sufficient to ensure a good segmentation of the coin even in presence of noise. The result of the segmentation is given in Figure 5 (b) with the following parameters: $\alpha = 3$, $\beta = 2$, $\gamma = 2$, $\Delta t = 0.5$, $\mu = 1$, $\mathcal{G} = 5$. The snaxel length was kept at 1 pixel by resampling of the snake during the convergence.

The third example of this subsection deals with the segmentation of an object whose a part of its contours is hidden by other objects (see Figure 6). In areas where the contours of the object to segment are hidden by another object (in our case the rings of Saturn hide some parts of the planet) the information provided by the edge detector is no more available and the convergence is entirely based on the intrinsic internal energy of the snake. That is, the snake provides us with a subjective contour illusion characterized by its intrinsic smoothness. However some artifacts appear at the intersection between the planet and the ring. They could certainly be removed increasing the value of the bending parameter (β). The snake parameters for this example were: $\alpha = 5$, $\beta = 2$, $\gamma = 2$, $\Delta t = 0.5$, $\mu = 1$, $\mathcal{G} = 5$. The

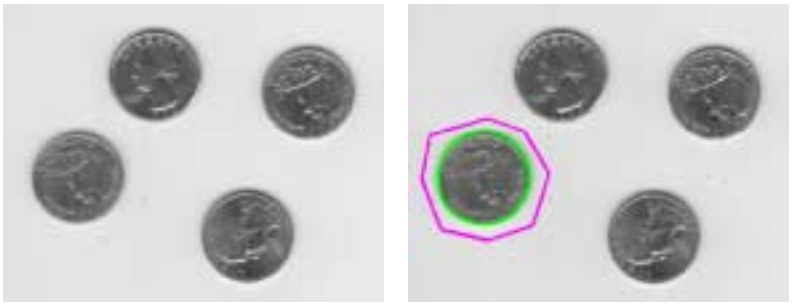

(a) (b)

Figure 4: (a) Original image. (Image *eight.tif* from the Image Processing Toolbox of MATLAB.) (b) Result of the segmentation by a classic snake of the coin situated in the lower left corner (green curve). The magenta curve represents the initial conditions (actually 8 discrete points connected by straight lines).

snaxel length was kept at 1 pixel by resampling of the snake during the convergence.

In the following part of the present section we are going to focus our attention on some poor properties of the basic snake. Improvements will be proposed in Subsections 4.2 and 4.3. First, because of its definition, the snake always tries to be smooth in order to minimize its internal energy (see Equation (2)). This property may be a great advantage especially when the images to process are strongly noisy, but this property becomes a disadvantage at corners where the snake should be second-order discontinuous. It is in contradiction with the model stated in Section 1 and the snake performances are very poor at these locations. However if the snake has a high enough resolution (i.e. if the distance between snaxels is small (≤ 1)) the smoothing effect is minimized (see for example Figure 7). Moreover if the sampling is done such that a snaxel is exactly situated at a corner the final result is satisfying even if the distance between snaxel is important (Figure 8). In more complicated cases such as shown in Figure 9, the classic snake provides with poor performances. Moreover the final solution strongly depends on the initial conditions and even with basic images, as those we are dealing with, the *right* convergence is not always reached (see Figure 9 (b)). On Figure 9 (c) another limitation of the classic snake is shown, that is, the active contour does not converge into concavities. The cases illustrated in Figure 9 (b) and (c) can be easily improved by introducing a new external force field called *gradient vector flow* (GVF) [10] instead of the simple force derived from the gradient (Subsection 4.2). In order to improve the behavior at corner, we propose a new approach based on the dynamic modification of the rigidity parameter (β). β is progressively decreased around a corner until reaching a null value at the exact corner location. Setting β to zero allows the snake to become second-order discontinuous and the develop a corner (see Subsection 4.3).

4.2 Gradient Vector Flow

The gradient vector flow (GVF) was originally introduced by Xu and Prince in [10] in order to improve some poor properties of the force field generated by the gradient operator:

- The gradient of an edge map $\nabla(-E'^{(i)}_{ext}(x,y))$ has vectors pointing toward the edges, which are normal to the edges at their locations

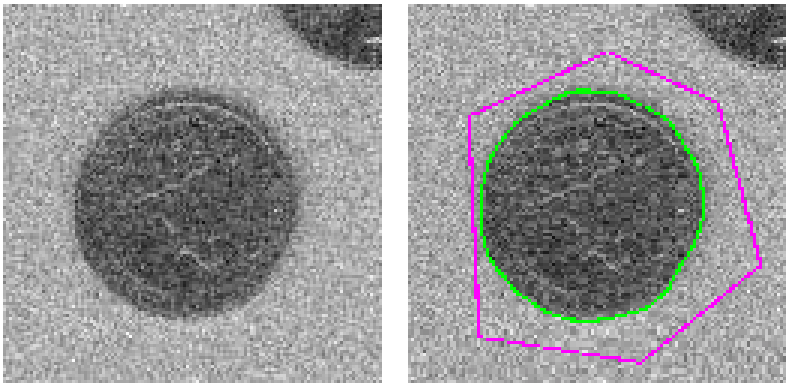

(a) (b)

Figure 5: (a) Original image for the second example. It consists in the same coin as above but in presence of an additive Gaussian noise (SNR = 12 dB). (b) Result of the segmentation by a classic snake (green curve). The magenta curve represents the initial conditions (actually 6 discrete points connected by straight lines).

Figure 6: Segmentation of the planet of Saturn. The snake algorithm provides us with a subjective contour illusion where the planet areas are hidden by its rings. (Magenta curve: initial contour, green curve: result of the segmentation.)

- These vectors generally have large magnitude only in the immediate vicinity of the edges
- In homogeneous regions where the image is nearly constant, $\nabla(-E'^{(i)}_{ext}(x,y))$ is nearly zero.

Although the first property is highly desirable, the last two properties are not. The second one induces a very small capture range and because of the third one, homogeneous regions will have no external forces. The overall approach is to use the force balance equation (20) and introduce a new external force field $\mathbf{F}^{(p)}_{ext} = \mathbf{v}(x,y)$, which is called gradient vector flow (GVF). The idea is based on the Helmholtz theorem which states that the most general static field can be decomposed into two components: an irrotational (curl-free) component and a solenoidal (divergence-free) component. In the classic case the static field is irrotational, since it is the gradient of a potential function. A more general static field can be obtained by allowing the possibility that it comprises both an irrotational and a solenoidal component. The

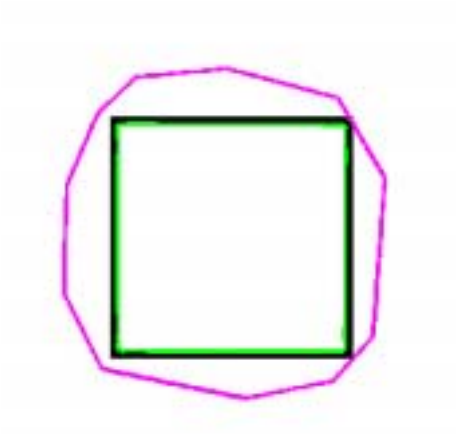

Figure 7: Segmentation of a square with the classic snake. The behavior at corners is good if the snake resolution is high enough (in this exemple, the distance between snaxel = 1 pixel).

GVF is defined so that $\mathbf{v}(x,y) = (u(x,y), v(x,y))'$ minimizes the energy functional

$$\varepsilon = \iint \mu(u_x^2 + u_y^2 + v_x^2 + v_y^2) + |\nabla f|^2 |\mathbf{v} - \nabla f|^2 \, dx \, dy$$

with

$$f(x,y) = -E'^{(i)}_{ext}(x,y)$$

as defined in Section 1.

[1]This variational formulation follows a standard principle, that of making the result smooth when there is no data. In particular, we see the when $|\nabla f|$ is small, the energy is dominated by sum of the squares of the partial derivatives of the vector field, yielding a slowly varying field. On the other hand, when $|\nabla f|$ is large, the second term dominates the integrand, and is minimized by setting $\mathbf{v}(x,y) = \nabla f$. This produces the desired effect of keeping $\mathbf{v}$ nearly equal to the gradient of the edge map when it is large, but forcing the field to be slowly-varying in homogeneous regions. The parameter μ is a regularization parameter governing the tradeoff between the first and second term in the integrand. (...) Using the calculus of variations, it can be shown that the GVF field can be found by solving the following Euler equations

$$\mu \nabla^2 u - (u - f_x)(f_x^2 + f_y^2) = 0$$
$$\mu \nabla^2 v - (v - f_x)(f_x^2 + f_y^2) = 0$$

where ∇^2 is the Laplacian operator. These equations provide further intuition behind the GVF formulation. We note that in a homogeneous region (where the image is constant), the second term in each equation is zero. Therefore, within such a region u and v are each determined by Laplace's equation, and the resulting GVF field is interpolated from the region boundary, reflecting a kind of competition among the vectors. This explain why GVF yields vectors that point into the concavities.

The introduction of the GVF instead of the gradient force provides two great advantages. The first advantage is the convergence of the snake into concavities (Figure 10 (a)) and the second one, a less sensibility to the initial conditions (Figure 10 (b)). Indeed, with the same initial conditions as in Figure 9 (c) the snake

Figure 8: Segmentation of a square with the classic snake. The behavior at corners is good even with a low snake resolution if a sampling is situated exactly at a corner position (distance between snaxel = 4 pixels). Each circle along the snake corresponds to a sampling. (Magenta curve: initial contour, green curve: result of the segmentation.)

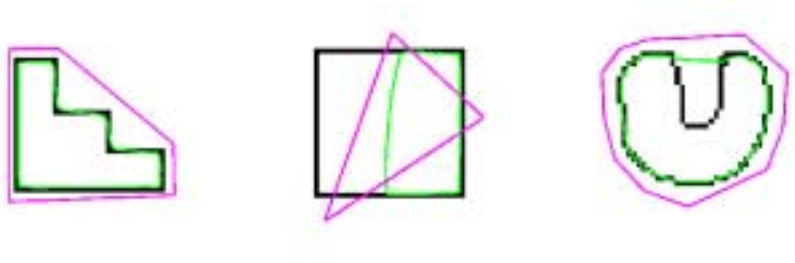

(a) (b) (c)

Figure 9: (a) Poor performances of the classic snake at corners. (b) Dependency of the classic snake on initial conditions. (c) The classic snake does not converge into concavities.

converges towards the *right* or at least the expected solution. The introduction of the GVF strongly improves the convergence of the classic snake towards the desired solution, but it also deteriorates the performances at corners. Although the classic snake is not designed for corner matching because of its intrinsic smoothness, the results can be quite satisfying if the snake resolution is sufficient. The snake behavior at corners in presence of the GVF is poorer than with the classic snake because of the diffusion effects explained in the previous paragraph. Figure 11 shows the field evolution around a corner in the gradient case (a) and in the GVF case (b). From the figure, it is obvious that in the latter case the field components diffuse the force and the corner location is not as well defined as in the classic case. This same effect is however highly desirable for the increasing of the capture range as well as for the convergence of the snake into concavities. The diffusion effect is illustrated in Figure 12.

[1] The next paragraph is cited from [10].

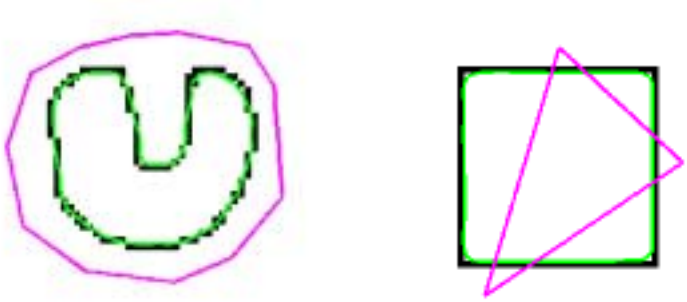

(a) (b)

Figure 10: Improvement due to the GVF introduction. (a) Convergence into concavities. (b) Smaller dependency on initial conditions. (Magenta curve: initial contour, green curve: result of the segmentation.)

As shown through the above examples, the GVF turns out to be very powerful, but it proves some lack of performance in presence of corners. It is thus not the universal solution to our problems and improvements of the snake behavior in presence of corners is presented in the next subsection.

4.3 Improvement at Corners

In that subsection, we present a new scheme that increases the snake performances in presence of corners. The basic idea is to relax the rigidity (β) around a corner and set it to zero at the exact corner location in order to allow the snake to become second-order discontinuous and thus to develop a corner. The equations (22.a) and (22.b) have to be solved taking into account the fact that β is not constant any more. It complicates the numerical implementation but the convergence time is not too much deteriorated.

The values of β are computed in a preprocessing step described as follow:

1. Detection of corners in the image
2. At each corner location, we associate a symmetric Gaussian distribution with a standard deviation of a few pixels (typically 2 - 3 pixels). This generates a new image which we refer to as $\mathcal{I}$.
3. $\mathcal{I}$ is normalized respective to its greater value, sign-inverted and finally 1 is added to the result ($\mathcal{I}' = 1 - \mathcal{I}/\max(\mathcal{I})$). The resulting image ($\mathcal{I}'$) is thus 1 everywhere except around the corners where it decreases according to a symmetric Gaussian distribution until 0 at the corner location.
4. Finally $\mathcal{I}'$ is multiplied by the value of β that the snake should have if β was constant.

We thus obtain a *map* of values of β where the rigidity is important everywhere but at corner locations. A typical map of β is shown in Figure 13. For the examples presented in this report, the corner locations were placed manually. This task can of course also be done by the mean of any corner detectors already existing in the image processing literature.

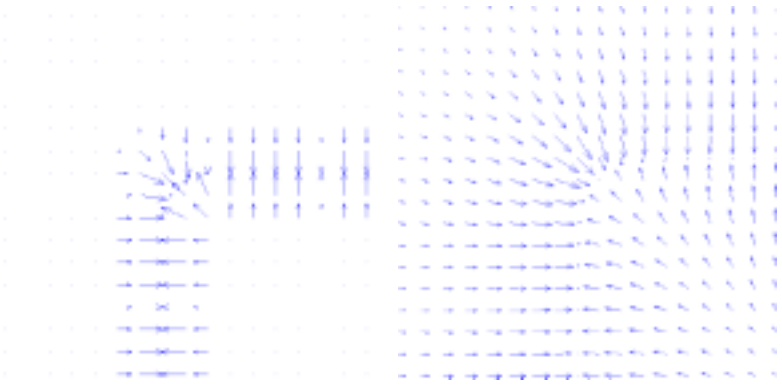

(a) (b)

Figure 11: Gradient external forces (a) and GVF external forces (b) around a corner location.

An comparison between the classic snake and the new method presented above is shown in Figure 14. The results are not as good as we could hope, but it is clear that around the corner locations the condition on the rigidity is relaxed and the curve tends to be second-order discontinuous. If we zoom in towards the *steps* in the middle of the image, we better see the contribution of the new method (see Figure 15). However due to the intrinsic smoothness of the snake and especially due to the elasticity term (α) the snake tries minimizing its length. The consequence of it is that the snake passes through the steps without being attracted by the corners. This can be improved by modifying the external energy of the snake. For example, a new energy field can be defined as the addition of the classic gradient field with the β map $\mathcal{I}'$ defined above. In that case both the external and internal energies of the snake will be very small around the corners and the snake will better approximate the edges to match. An illustration is given in Figure 16. Comparing Figure 16 (a) and (b), it is obvious that the improvement due to the new external energy is really worthwhile. However, the snake remains too smooth at the first and third corner of the step. This situation can again be improved if the variation of β is introduced as above. Figure 16 (c) shows that the corners are well matched as well as for their locations as for the second-order discontinuity of the curve.

5 Conclusion and Outlook

The first part of this work deals with the complete derivation of the motion equations of the classic snake as introduced by Kass *et al.* [4]. We propose an approach based on the mechanics of the deformable solid and we then rely on the snake parameters with some physical values. We show that the membrane-like and thin plate-like interpretations are justified. In the last chapter we give some examples of edge detection and we show some limitations of the basic method. Many solutions are then proposed in order to improve the snake convergence and the poor performances in presence of corner. We especially introduce a new convergence scheme based on the variation of the rigidity (β) in function of the image content. We also propose a modification of the external energy which better attracts the snake at a corner location. The combination of both new methods seems to produce a real improvement in the convergence quality without complicating the numerical

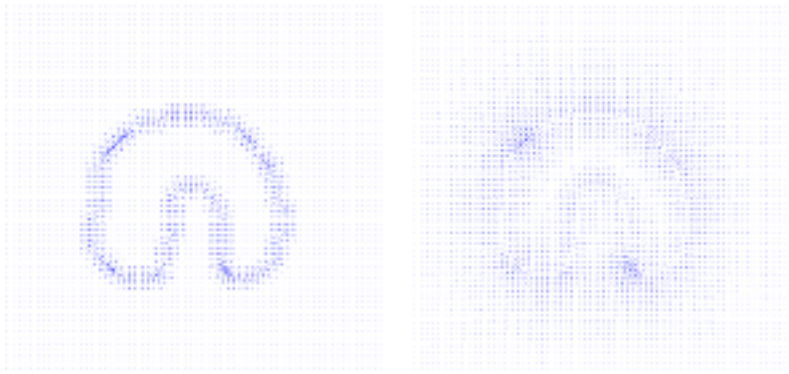

(a) (b)

Figure 12: Gradient external forces (a) and GVF external forces (b). In the GVF case, the capture range is wider and due to the diffusion process, the vectors points into the concavity.

implementation and thus without degrading the computing time too much.

This deep study on the basic snake model shows that these types of active contours can be very efficient and robust. The snake has the potential advantage of robustness to image and noise due to the smoothness constraints and the integration of energy along the entire length of the snake. However, the following difficulties may arise when using the basic or improved algorithm presented in this report.

- α and β depend too much on the image to process
- The convergence is relatively slow due to the high number of snaxels that defined the curve
- It is difficult to control the snake behavior during the evolution
- The snake is represented by a sequence of separated points which offers poor resolution and accuracy. An increase in the number of points does not always lead to better results.

All these reasons imply the need for a new and continuous description of the curve. We believe that a spline (or B-spline) representation as well as a new expression of the smoothness constraint are necessary. That is why we are proceeding our work in the directions proposed in [8] or [2]. A B-spline representation allows the local control of the snake evolution and a continuous description the resampling of the different control points. For example, a redistribution of the control points has the great advantage to increase the snake resolution at hard corner locations without increasing the number of snaxels and thus the computation time.

References

[1] K. Arbenz and A. Wohlhauser. *Compléments d'analyse*, volume 2 of *Méthodes mathématiques pour l'ingénieur*. Presses Polytechniques et Universitaires Romandes, Lausanne, Switzerland, 1993.

[2] P. Brigger, J. Hoeg, and M. Unser. B-spline snakes: a flexible tool for parametric contour detection. *IEEE Transactions on Image Processing*, in press.

(a) (b)

Figure 13: (a) Original image. (b) Superposition of the β map and the original image. We can see that the β map is minimal at the corner locations, increases around the corners (according to a symmetric Gaussian distribution) and is maximal otherwise.

[3] C. Gruber and W. Benoit. *Mécanique Générale*. Presses Polytechniques et Universitaires Romandes, Lausanne, Switzerland, 1998.

[4] M. Kass, A. Witkin, and D. Terzopoulos. Snakes: Active contour models. *International Journal of Computer Vision*, pages 321–331, 1988.

[5] F. Leymarie and M. D. Levin. Tracking deformable objects in the plane using an active contour model. *IEEE Transactions on Pattern Analysis and Machine Intelligence*, 15(6):617–634, June 1993.

[6] S. Lobregt and M. A. Viergever. A discrete dynamic contour model. *IEEE Transactions on Medical Imaging*, 14(1):12–24, March 1996.

[7] I. S. Sokolnikoff. *Mathematical Theory of Elasticity*. Krieger Publishing Compagny, Malabar, Florida, 1983.

[8] M. Wang, J. Evans, L. Hassebrook, and C. Knapp. Multistage, optimal active contour model. *IEEE Transactions on Image Processing*, 5(11):1586–1591, November 1996.

[9] E. W. Weisstein. *Curvature*. http://mathworld.wolfram.com/Curvature.html, 2000.

[10] C. Xu and J. L. Prince. Snakes, shapes, and grandient vector flow. *IEEE Transactions on Image Processing*, 7(3):359–369, March 1998.

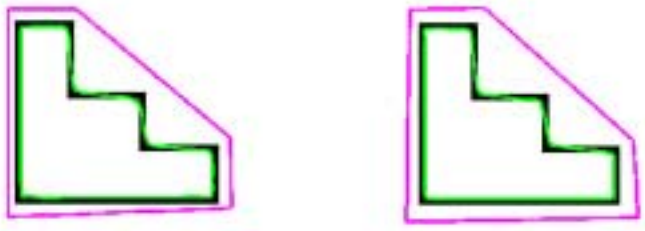

(a) (b)

Figure 14: (a) Basic snake. (b) Basic snake with a non constant rigidity ($\beta = \beta(x,y)|_{snake}$). (Magenta curve: initial contour, green curve: result of the segmentation.)

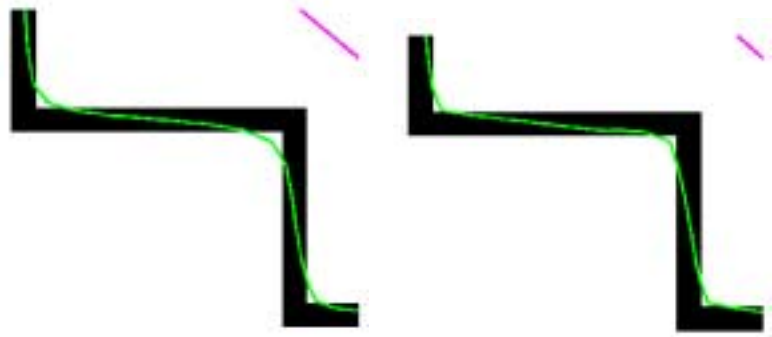

(a) (b)

Figure 15: (a) Basic snake. (b) Basic snake with a non constant rigidity ($\beta = \beta(x,y)|_{snake}$). Around the corners, the snake in (a) is smoother than in (b) as expected.

(a) (b) (c)

Figure 16: (a) Basic snake. (b) Modified energy field *without* corner detection. (c) Modified energy field *with* corner detection.